Journal of Materials Chemistry A

ROYAL SOCIETY OF CHEMISTRY

PAPER

View Article Online
View Journal | View Issue

Open Access Article. Published on 06 January 2026. Downloaded on 5/24/2026 8:23:32 PM. This article is licensed under a Creative Commons Attribution-NonCommercial 3.0 Unported Licence.

Check for updates

Cite this: *J. Mater. Chem. A*, 2026, **14**, 5935

Hydroxylammonium nitrate: synthesis, cocrystals, and properties

Andrew J. Bennett, [a] Haley R. Froberg, [a] Michael K. Bellas, [b] Leila M. Foroughi [a] and Adam J. Matzger *[ac]

Received 10th October 2025
Accepted 5th January 2026

DOI: 10.1039/d5ta08279j

rsc.li/materials-a

Hydroxylammonium nitrate (**HAN**) is a high-performing, less-toxic alternative to hydrazine in liquid propellants. **HAN** also possesses many desirable qualities for use as an oxidizer in solid propellant formulations, where a chlorine-free replacement for ammonium perchlorate is urgently required; however, the extreme hygroscopicity of **HAN** precludes it from consideration for this role. Ionic cocrystallization, the combination of a salt and a neutral molecular solid within a crystal lattice, is demonstrated here to overcome this limitation for the first time. Solid **HAN**, synthesized *via* salt metathesis in ethanol and purified *via* sublimation, provides an ideal starting point for cocrystallization. Melt fusion at 50 °C readily generated the first examples of **HAN** cocrystals. The cocrystals feature dramatically reduced hygroscopicity, stabilizing **HAN** against ambient moisture for the first time. Three of nine cocrystals were formed between **HAN** and molecules with proposed or realized applications in propellants or explosives, and these possess calculated specific impulse and detonation velocity exceeding those of both **HAN** and the respective coformer molecules.

Introduction

In liquid rocket propellants, hydrazine and its derivatives are widely used for in-space monopropellant propulsion systems as well as certain in-atmosphere bipropellant launch vehicles.[1] However, these compounds pose severe health hazards (acute and chronic) upon exposure,[2,3] eliciting substantial research promoting less hazardous "green" replacement fuels.[4–6] Hydroxylammonium nitrate (**HAN**) (Fig. 1) has received significant attention as an alternative to hydrazine in the next generation of liquid propellants thanks to its increased oxygen content and reduced toxicity.[7,8] **HAN** has been applied for in-space propulsion[9–11] and is being investigated as an oxidizer in electrically ignited gelled propellant formulations.[12,13] Parallel to the search for less hazardous liquid propellants, a similar search is ongoing in the realm of solid propellants where toxic and environmentally damaging ammonium perchlorate (**AP**) continues to reign as the state-of-the-art oxidizer.[14–16] In spite of its strong qualifications as a component in liquid propellants, oxygen content on-par with **AP** and existing production infrastructure in the United States, **HAN** has yet to become a serious contender as an **AP** replacement in composite formulations. **HAN** is almost categorically disqualified for its extreme hygroscopicity, which is such that it deliquesces (forms a solution with atmospheric moisture) nearly immediately at ambient conditions. Further, the solid-state properties of **HAN** are poorly studied in general,[17] especially in comparison to other proposed **AP** alternatives including ammonium nitrate (**AN**) and ammonium dinitramide (**ADN**).[18–21]

Maturing **HAN** to the point of serious consideration as a composite propellant component requires overcoming its hygroscopicity and establishing the ground-level characterization required for safety evaluation of the solid form. Towards the former, ionic cocrystallization (the combination of a salt and a neutral molecular solid in a crystal lattice) has been established as an effective route for reducing the hygroscopicity of oxidizing salts.[22,23] With respect to the latter, the hazards and

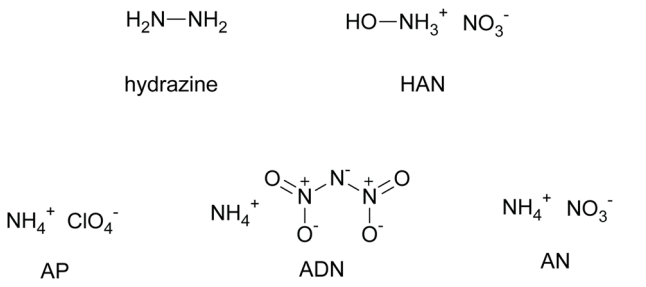

Fig. 1 Chemical structures of hydrazine and oxidizing salts: hydroxylammonium nitrate (**HAN**), ammonium perchlorate (**AP**), ammonium dinitramide (**ADN**), and ammonium nitrate (**AN**).

[a]*Department of Chemistry, University of Michigan, 930 North University Ave, Ann Arbor, MI 48109, USA. E-mail: matzger@umich.edu*

[b]*China Lake NAWCWD, 1 Admin Circle, China Lake, CA 93555, USA*

[c]*Macromolecular Science and Engineering Program, University of Michigan, Ann Arbor, MI 48109, USA*

Open Access Article. Published on 06 January 2026. Downloaded on 5/24/2026 8:23:32 PM. This article is licensed under a Creative Commons Attribution-NonCommercial 3.0 Unported Licence.

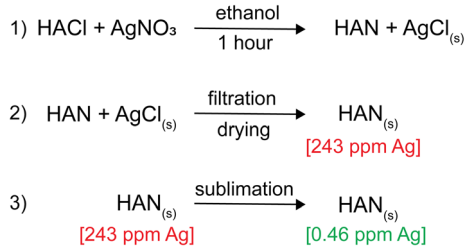

Scheme 1 Reaction scheme for synthesis and purification of **HAN**.

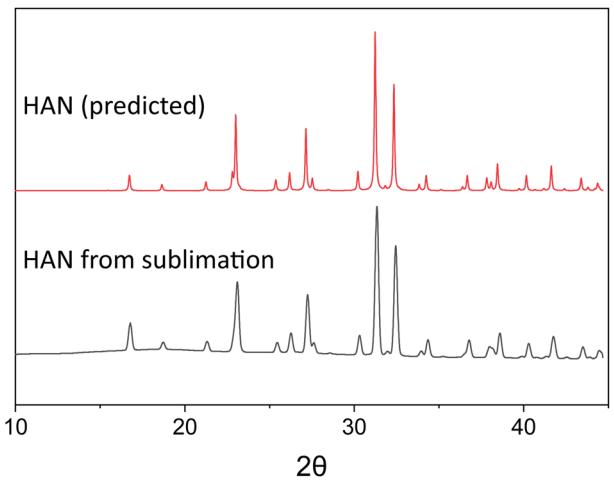

Fig. 2 Experimental **HAN** powder pattern compared to the simulated powder pattern (ICSD 60990).

challenges associated with generating solid-phase **HAN** have long encumbered characterization efforts.[24–27] This, coupled with the fact that cocrystallization relies on principals of supersaturation requiring careful selection of the ideal solvent(s) and saturation levels to generate and harvest the target cocrystal,[28] spurred our development of a simpler and safer solid-phase **HAN** synthesis. Effective strategies for **HAN** cocrystallization are presented and utilized to generate the first examples of **HAN** cocrystals, most of which show dramatically reduced hygroscopicity relative to the salt. Three cocrystals in the set additionally possess promising energetic properties, representing a significant stride towards enabling **HAN** incorporation in composite propellants.

Results and discussion

HAN was synthesized by combining hydroxylammonium chloride with silver nitrate in anhydrous ethanol to generate a solution of **HAN** while precipitating silver chloride (Scheme 1). This solution can be filtered to separate bulk silver chloride and then dried under vacuum or N_2 flow to yield anhydrous **HAN**. Contamination with silver chloride or excess silver nitrate is readily detected by a slight darkening of the white solid after extended exposure to ambient light or brief exposure to an intense light source which accelerates the decomposition of silver chloride to silver metal and chlorine gas. Because metal ions are known to catalyze the decomposition of **HAN**,[29,30] the solid product was purified using sublimation. This process generates pure solid **HAN** in 97% yield at the 1 g scale. The sublimate was characterized with powder X-ray diffraction (PXRD) and matches well with the simulated pattern of **HAN** (Fig. 2). Microwave plasma atomic emission spectroscopy (MP-AES) was used to quantify the total silver contamination in **HAN** samples before and after sublimation. While an official target for metal contaminant levels in **HAN** has not been published, a de facto limit of 5 ppm in 24 wt% **HAN** solutions is referenced in a 1990 report by the Olin Corporation on an army contract for the synthesis of pure **HAN**.[31] As reported by MP-AES our sublimated **HAN** contains 0.46 ppm silver at 100% concentration, translating to 0.11 ppm in a 24 wt% solution, well below the 5 ppm target. Prior to sublimation, the **HAN** contains 239 ppm silver, or 57.3 ppm in a 24 wt% solution. We expect that purification by sublimation is also a useful strategy for other **HAN** syntheses which employ hydroxylammonium sulfate and nitrate salts of barium or calcium. Like silver

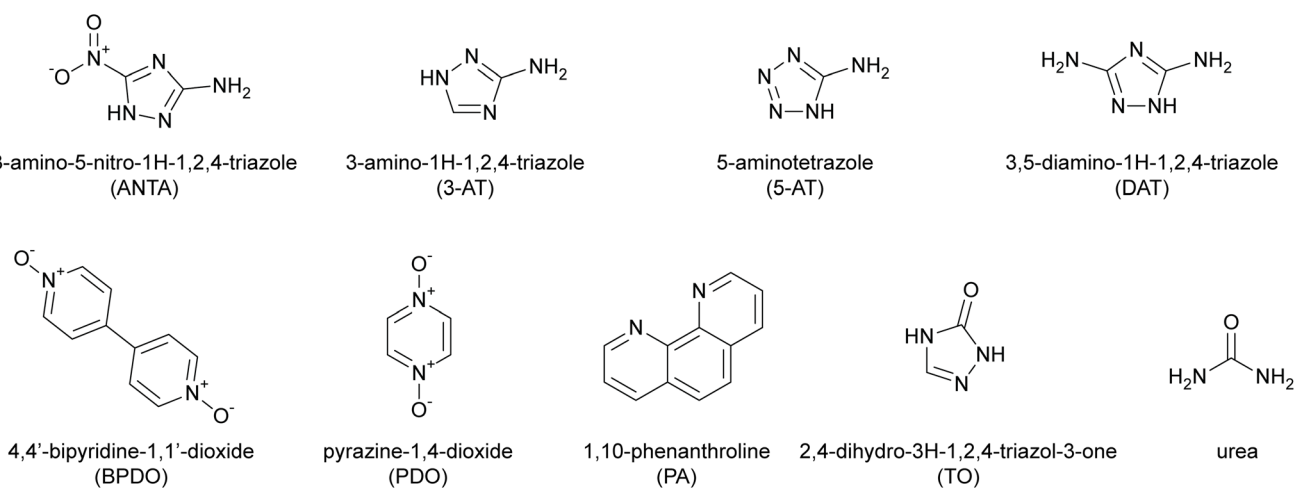

Fig. 3 Chemical structures of nine coformers successfully cocrystallized with **HAN**.

 This journal is © The Royal Society of Chemistry 2026

Open Access Article. Published on 06 January 2026. Downloaded on 5/24/2026 8:23:32 PM.
This article is licensed under a Creative Commons Attribution-NonCommercial 3.0 Unported Licence.

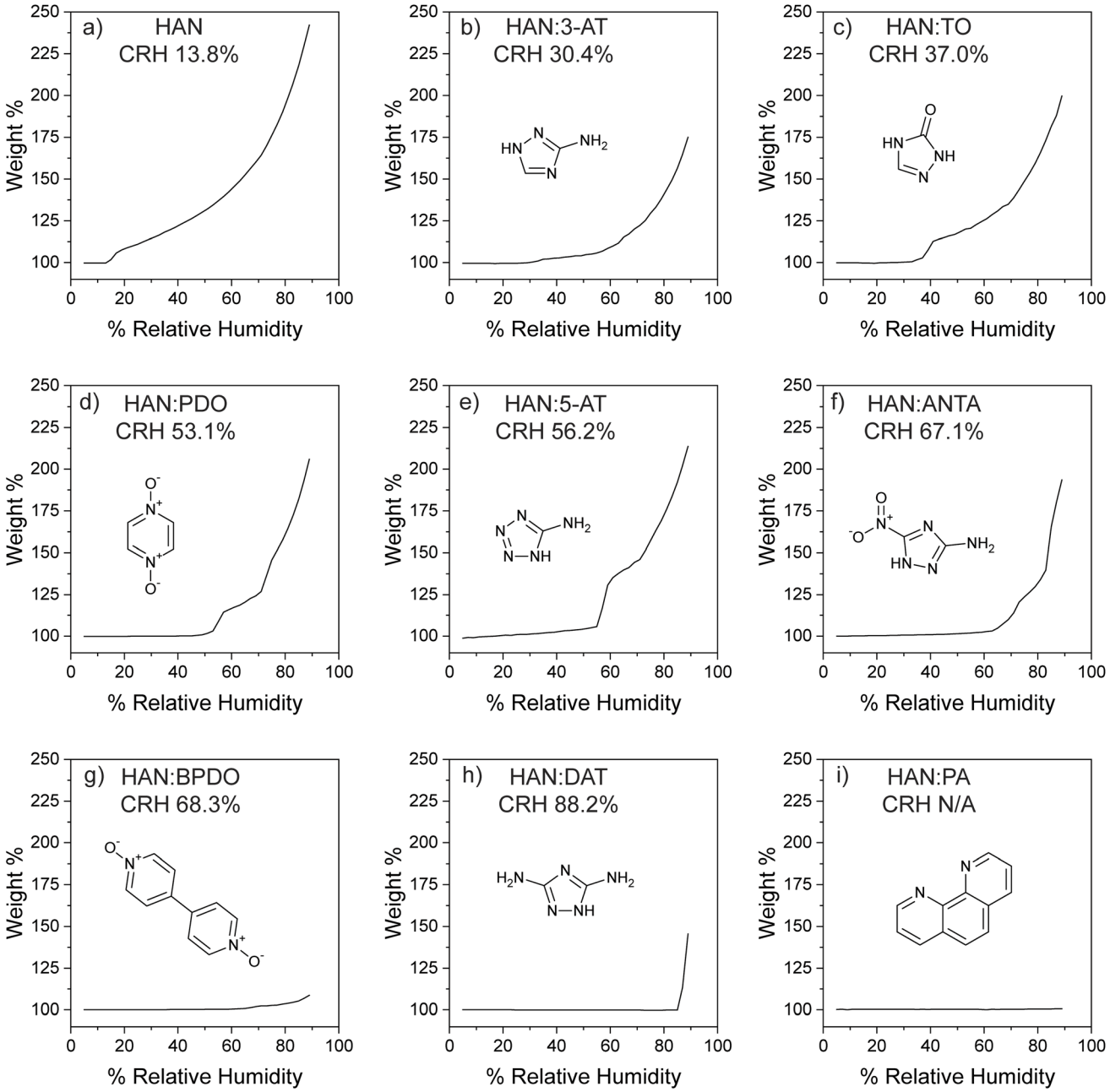

Fig. 4 DVS plots of (a) **HAN**, and the cocrystals (b) **HAN**:**3-AT**, (c) **HAN**:**TO**, (d) **HAN**:**PDO**, (e) **HAN**:**5-AT**, (f) **HAN**:**ANTA**, (g) **HAN**:**BPDO**, (h) **HAN**:**DAT**, and (i) **HAN**:**PA**.

chloride, barium sulfate and calcium sulfate have negligible vapor pressure[32,33] and should remain as solid residue during sublimation, especially with the gentle conditions employed in this work.

The severe hygroscopicity of pure **HAN** precludes its use in traditional composite propellants and is a significant impediment to research on the properties of its anhydrous form. Cocrystallization has been shown to reduce the hygroscopicity of other chlorine-free oxidizing salts **AN** and **ADN** and has therefore been applied to **HAN** in the present study. Solid **HAN** is ideal for rapid cocrystal discovery. A low melting point of around 48 °C makes **HAN** an excellent candidate for melt fusion (nomenclature surrounding melt techniques varies[34–36]), a powerful cocrystallization technique in which the molten form of the low-melting coformer (cocrystallization partner) solvates and fuses with a solid coformer, which bypasses the need for individual design of solvent systems. Using melt fusion, a set of **HAN** cocrystals with nine different coformers was generated as the first example of **HAN** cocrystallization in the literature (Fig. 3). Raman spectroscopy was used to identify successful cocrystallization by shifts in the known peaks of **HAN** and the coformers (Fig. S12). In every case, single crystals of sufficient quality for structure determination by single crystal X-ray diffraction (SCXRD) were formed directly by melt fusion.

Open Access Article. Published on 06 January 2026. Downloaded on 5/24/2026 8:23:32 PM.
This article is licensed under a Creative Commons Attribution-NonCommercial 3.0 Unported Licence.

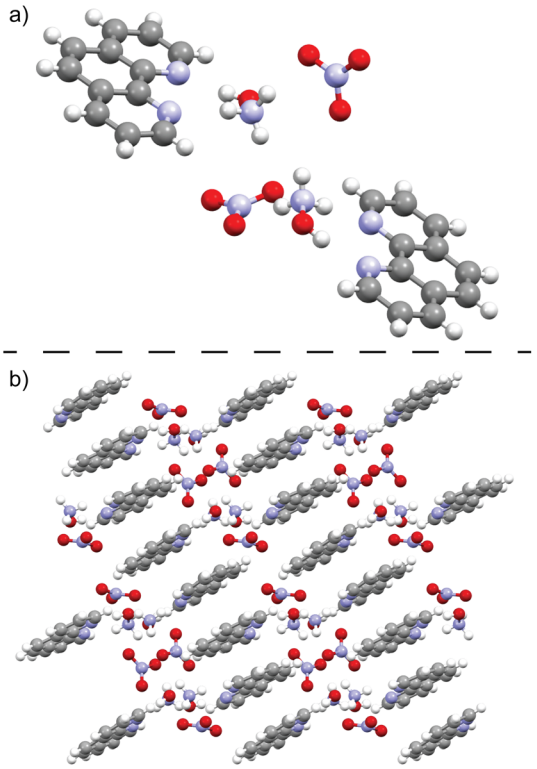

Fig. 5 (a) Asymmetric unit of HAN:PA and (b) crystal packing structure of HAN:PA.

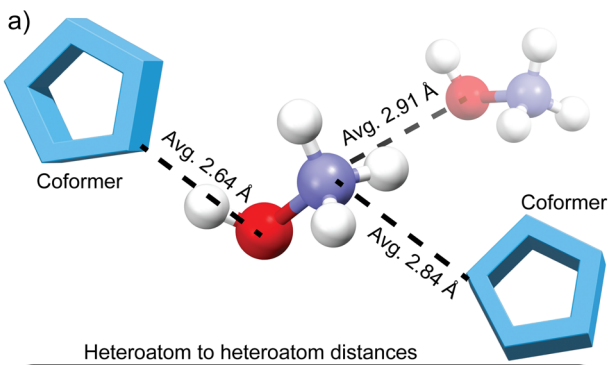

Heteroatom to heteroatom distances

b)	Avg. H-bond distance	Avg. vdW overlap
hydroxyl ····· coformer	2.64 Å	0.466 Å
ammonium ····· coformer	2.84 Å	0.405 Å
hydroxyl ····· ammonium	2.91 Å	0.253 Å

Fig. 6 (a) Illustration depicting the average hydrogen bond distances between hydroxylammonium and the coformers and (b) average van der Waals overlap of the same interactions. All distances are between heteroatoms.

However, melt fusion is best employed as a screening technique, and in some cases once a cocrystal had been identified, recrystallization by evaporation or slurry techniques was necessary to produce higher quality crystals for publication-quality structures. All nine cocrystals are also accessible by grinding **HAN** with the coformers under a dry atmosphere; although laborious as a screening technique, this was our preferred method for obtaining pure samples for thermal analysis. The purity of the samples was verified with powder X-ray diffraction (Fig. S10).

Eight out of nine cocrystals have drastically reduced hygroscopicity compared to **HAN**, qualitatively apparent by their continued solidity at ambient. These cocrystals are the first instances of solid **HAN** showing stability towards atmospheric moisture. **HAN**:urea, which deliquesces under ambient conditions, was not studied further. Dynamic vapor sorption (DVS) was used to quantify the hygroscopicity of the remaining eight cocrystals and **HAN** by determining the critical relative humidity (CRH) for each. The CRH is the relative humidity at which the sample begins to deliquesce (Fig. 4).

To our knowledge the hygroscopicity of solid **HAN** (CRH 13.8%) has not been quantified previously. Most of the cocrystals have CRH values between 30–88%, a significant reduction in hygroscopicity which allows these materials to stay dry within typical laboratory conditions. This consistent reduction in hygroscopicity, even in the presence of hydrophilic coformers, argues for a low lattice energy of **HAN** leading to anomalously high hygroscopicity. This notion is supported by its relatively low melting temperature relative to hydroxylammonium chloride (48 °C for **HAN** *versus* 155 °C for hydroxylammonium chloride) as well as significantly reduced volatility of the cocrystals relative to **HAN** (*vide infra*). Notably, **HAN:PA** did not deliquesce at any point during the experiments. This can potentially be explained by the crystal packing structure of the cocrystal, in which hydrophilic **HAN** is mostly caged in by bulky hydrophobic phenanthroline while participating in hydrogen bonding interactions with the sp^2 nitrogens of the latter (Fig. 5). The cocrystals were also assessed for phase stability under humid conditions by examining the powder X-ray patterns of the samples after DVS experiments (Fig. S11), and most reformed after drying the solution resulting from deliquescence (*i.e.* pure cocrystal with no hydrates or coformers) with three exceptions. After exposure to 90% relative humidity: **HAN:5-AT** is partially converted to 5-aminotetrazole monohydrate, **HAN:DAT** breaks down into a mixture of cocrystal and diaminotriazole monohydrate, and **HAN:3-AT** decomposes to form a nitrate salt of the coformer 3-aminotriazole.

Coformers for this study were selected based on our previous work with hydroxylammonium chloride (HACl), in which we found that hydroxylammonium is prone to hydrogen bonding with *N*-oxides and sp^2 nitrogen atoms, with the hydroxyl functionality consistently forming closer contacts (greater van der Waals overlap) with the coformer molecules than the ammonium functionality.[37] The reliability of these interactions makes them an ideal choice for **HAN** cocrystal design, and therefore every coformer in the present work features *N*-oxide or sp^2 nitrogen functionality. Consistent with our previous work involving HACl, in **HAN** cocrystals the hydroxylammonium cation donates one or more hydrogen bonds to an *N*-oxide or sp^2 nitrogen of the coformer molecule and the hydroxyl functionality forms closer contacts with coformers than the ammonium functionality (Fig. 6). In addition to its two hydrogen bond

 This journal is © The Royal Society of Chemistry 2026

Open Access Article. Published on 06 January 2026. Downloaded on 5/24/2026 8:23:32 PM. This article is licensed under a Creative Commons Attribution-NonCommercial 3.0 Unported Licence.

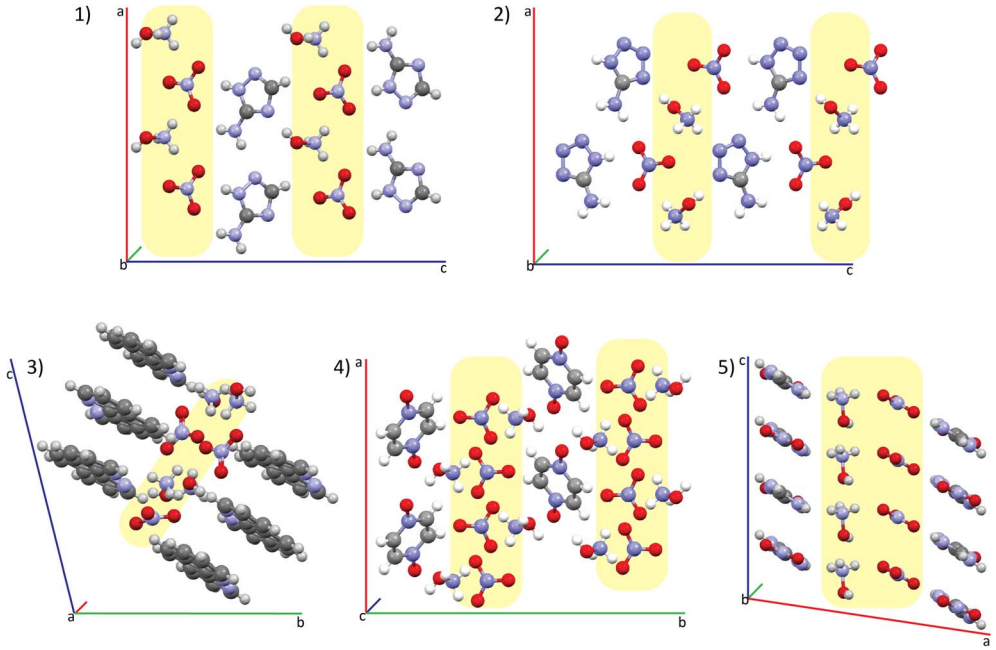

Fig. 7 Lamellar packing structures of (a) **HAN**:**3-AT**, (b) **HAN**:**5-AT**, (c) **HAN**:**PA**, (d) **2HAN**:**PDO**, and (e) **HAN**:**ANTA**. Salt lamellae are highlighted.

Table 1 Calculated detonation velocity (V_d), detonation pressure (P_{cj}), specific impulse (I_{sp}), oxygen balance (OB_{CO}), and density (ρ) for three energetic **HAN** cocrystals. **HAN** and RDX are included for comparison

	V_d (km s^{-1})	P_{cj} (GPa)	I_{sp} (s)	OB_{CO} (%)	ρ (g cm^{-3})
2HAN:PDO	8.21	25.8	247	0.00	1.67
HAN:ANTA	8.83	30.8	242	3.55	1.77
HAN:5-AT	8.98	29.6	236	−4.42	1.71
HAN	7.50	23.8	149	33.0	1.84
ANTA	8.33	30.3	207	−18.6	1.820
RDX	8.84	35.8	266	0.00	1.82

donating functionalities, the hydroxylammonium cation is capable of simultaneously accepting hydrogen bonds *via* lone pair electrons on the oxygen atom. This interaction appears to occur preferentially with itself. In six of nine cocrystals, hydroxylammonium accepts a hydrogen bond from the ammonium functionality of an adjacent hydroxylammonium cation. However, in none of the **HAN** cocrystals reported here does the hydroxyl functionality accept a hydrogen bond from a coformer molecule. Among the coformers selected for screening are six which were previously found to cocrystallize with HACl; **BPDO**, **PDO**, **DAT**, **PA**, isoquinoline *N*-oxide, and 4-picoline *N*-oxide. Of those six, four successfully cocrystallized with **HAN**, while two (isoquinoline *N*-oxide and 4-picoline *N*-oxide) did not. Isoquinoline *N*-oxide is protonated by **HAN** to form a nitrate salt whereas 4-picoline *N*-oxide reacts on contact with **HAN** to yield a liquid. HACl cocrystals are, therefore, a fair predictor for **HAN** cocrystal formation; however, subtleties arising from pK_a differences (chloride *versus* nitrate) must be considered.[38] Four of nine cocrystals feature lamellar architecture, a crystal packing motif defined by alternating sheets of salt and coformer "sandwiched" and extending infinitely along two axes (Fig. 7). Previous work has explored salt lamellae as a potential route towards achieving variable salt stoichiometry in ionic cocrystals,[39] although no examples of varied stoichiometry for a given coformer were discovered for the cocrystals featuring lamellar architecture in the present work.

Three of the cocrystals in this set warrant closer examination as potentially promising energetic materials: **HAN:ANTA**, **HAN:5-AT**, and **2HAN:PDO**. 3-Amino-5-nitro-1*H*-1,2,4-triazole (**ANTA**) is an insensitive high explosive that has attracted significant attention for its potential applications in insensitive munitions (IMs) and as a precursor for a variety of other energetic molecules.[40,41] **5-AT** is a high-energy nitrogen-rich heterocycle with demonstrated applications as a fuel in liquid and gelled propellant formulations, some of which also include **HAN**.[42–44] **PDO** is a common coformer in energetic cocrystals due to its high energy content and powerful hydrogen bond accepting capability.[45,46] Energetic performance properties were calculated using CHEETAH 7.1 thermochemical analysis software (Table 1). The calculated detonation velocities for the cocrystals are comparable to, or in the case of **HAN:5-AT**, slightly exceed that of the benchmark explosive hexahydro-1,3,5-trinitro-1,3,5-triazine (RDX). Oxygen balance (OB_{CO}), which compares the oxygen content of a given chemical or formulation to the amount required for its complete oxidation, is slightly negative (oxygen deficit) for **HAN:5-AT**, neutral for **2HAN:PDO**, and slightly positive (oxygen excess) for **HAN:ANTA**. Using an in-house drop height apparatus described in previous work,[47] impact sensitivity was determined for the first time for solid **HAN** and compared to that of the cocrystals and coformers. Impact sensitivity is here described as Dh_{50}, the height from which a dropped weight will cause the sample to detonate 50% of the time. Anhydrous **HAN** is mildly sensitive to impact (Dh_{50}

Open Access Article. Published on 06 January 2026. Downloaded on 5/24/2026 8:23:32 PM.
This article is licensed under a Creative Commons Attribution-NonCommercial 3.0 Unported Licence.

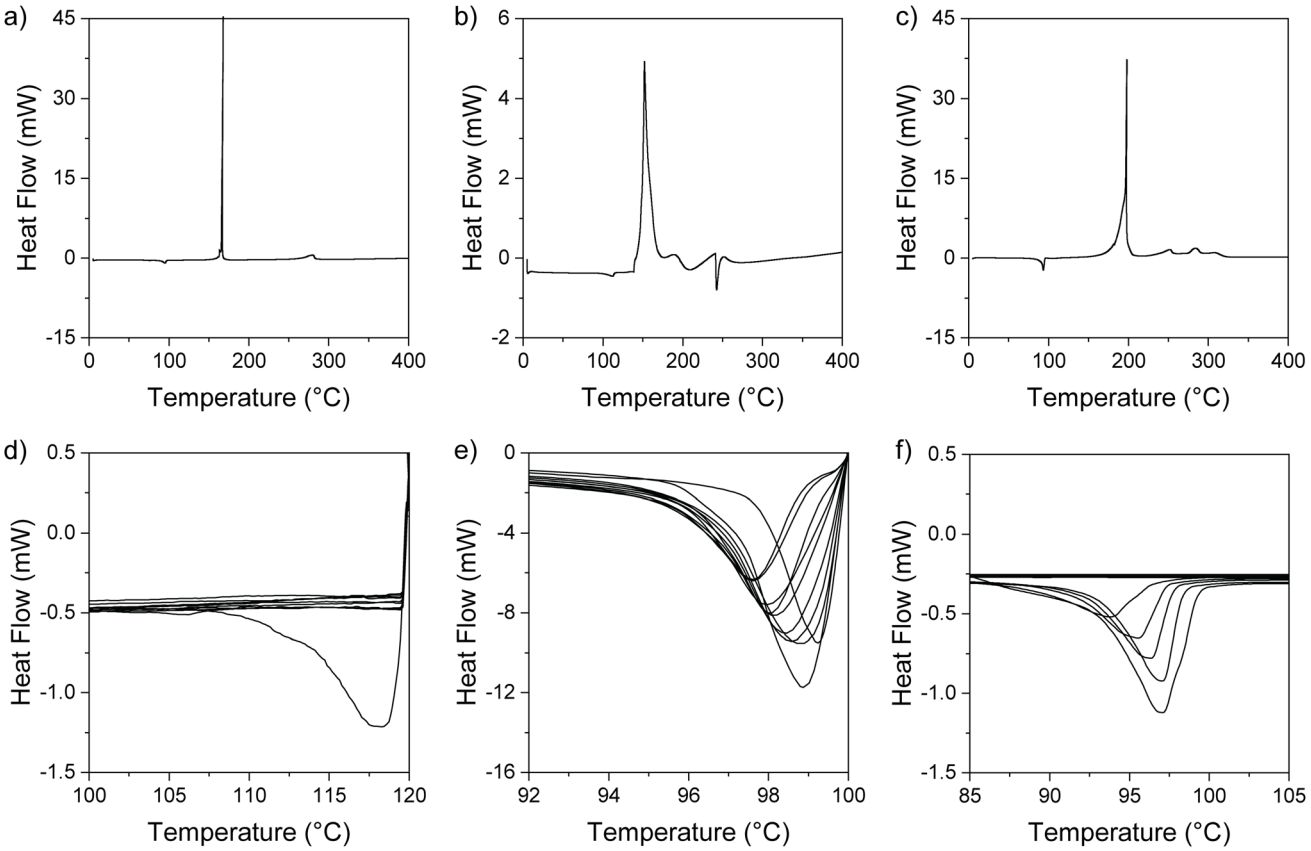

Fig. 8 DSC traces for (a) HAN:ANTA, (b) 2HAN:PDO, and (c) HAN:5-AT. Cyclic traces are depicted for (d) HAN:ANTA, (e) 2HAN:PDO, and (f) HAN:5-AT.

110 cm) and all three coformer molecules are insensitive to the limits of our apparatus (141 cm). **HAN:ANTA** is also insensitive to the limits of the apparatus, but **HAN:5-AT** (Dh_{50} 49 cm) and **2HAN:PDO** (Dh_{50} 38 cm) are drastically more sensitive than either mildly sensitive **HAN** or the insensitive coformers. Particular caution must be observed with **2HAN:PDO** which occasionally detonated from drop heights as low as 19 cm, within the range of primary explosives. Although only a few have been reported previously, this result is unique among energetic ionic cocrystals. Previous examples of sensitive ionic cocrystals (**2ADN:PDO**, **2ADN**:DNBT, **AP**:1HT)[23,48,49] contain at least one component with high impact sensitivity, and the sensitivity of the resulting cocrystals is similar to the sensitive component(s) rather than significantly increased. This work complements earlier findings on an energetic cocrystal less sensitive than either component (DADP:TITNB).[50]

The low melting point of anhydrous **HAN** may present another potential barrier to incorporation in solid formulations. Therefore, differential scanning calorimetry (DSC) was used to assess the thermal properties of the cocrystals (Fig. 8). All three energetic ionic cocrystals feature elevated melting points around 100 °C, above typical operating temperatures and well below their respective decomposition points. The potential for melt casting capability warranted further study of the cocrystal melting behavior. Each cocrystal was repeatedly cycled from 25 °C to just above its respective melting point to assess the stability of the molten cocrystal. In each case the melting point shifts with every cycle, indicating some instability and potential chemical degradation of the cocrystal. An optical melting temperature apparatus was then used to inspect the melting points visually. Upon reaching the supposed melting temperature, the cocrystals appear "wet" and partially melted but do not melt fully. At this point we suspected that **HAN** was melting out of the cocrystals at elevated temperatures and investigated the matter with thermogravimetric analysis (TGA). The cocrystals were held at 100 °C under continuous N_2 flow for 48 hours (Fig. S15). Initially, the samples lost mass rapidly (3–5 wt% per hour) but stabilized in the latter half of the experiment, supporting the idea that **HAN** is being liberated from the cocrystals and decomposing or vaporizing. PXRD analysis of the same samples after TGA experiments confirm that this is the case. Although not reported previously, solid **HAN** is highly volatile as evidenced by the ease of sublimation in this work. Previous work has demonstrated the effectiveness of cocrystallization in suppressing the volatility of energetic coformers, and so isothermal TGA experiments were then carried out at 80 °C and 60 °C for 10 hours to gain a more complete picture of the thermal stability of the cocrystals (Fig. 9). Mass loss rates at 80 °C are close to 1% per hour for all three cocrystals. At 60 °C, mass loss occurs at less than 0.1% per hour for each cocrystal.

 This journal is © The Royal Society of Chemistry 2026

Open Access Article. Published on 06 January 2026. Downloaded on 5/24/2026 8:23:32 PM.
This article is licensed under a Creative Commons Attribution-NonCommercial 3.0 Unported Licence.

a)

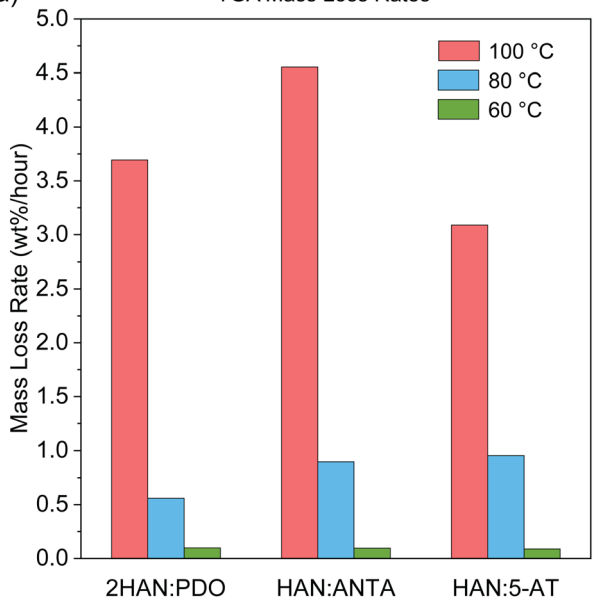

b) 60 °C Vacuum Mass Loss Rates

	Final Weight (%)	Mass Loss Rate (wt%/hr)
HAN:ANTA	91.4	0.36
HAN:5-AT	48.5	2.15
2HAN:PDO	37.8	>2.69
HAN	0.0	>4.17

c)

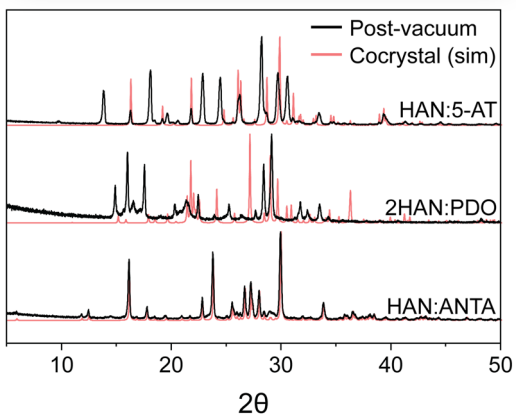

Fig. 9 (a) Bar plot showing mass loss rates of the energetic cocrystals during TGA experiments at 100 °C, 80 °C, and 60 °C. (b) Table of final mass percent and mass loss rates for the energetic cocrystals and **HAN** when held at 60 °C under vacuum for 24 hours, and (c) PXRD patterns of the samples after the vacuum experiment.

Inclusion of **HAN** as a comparison point proved difficult for TGA measurements, where uptake of atmospheric moisture prior to data collection threatens to skew the results of the experiment. Therefore a similar experiment was performed at elevated temperature in a sealed vacuum chamber where **HAN** can be more easily included. **HAN** and the energetic cocrystals were held at 60 °C under vacuum for 24 hours. The initial and final masses of the samples were compared to calculate the rate of mass loss. **HAN** was observed to vaporize completely in under 30 minutes. Aside from **2HAN:PDO**, the cocrystals show a marked improvement over **HAN** with a twofold suppression of volatility in the case of **HAN:5-AT** and nearly twelvefold for **HAN:ANTA**. These calculations were made with the minimum possible mass loss rate of **HAN** across the entire 24 hour experiment; taking into account the fact that **HAN** had visually vaporized entirely within 30 minutes, the actual improvement is likely many times greater.

Conclusion

Solid anhydrous **HAN** has been synthesized in one step from commercial reagents and purified via sublimation. This method is likely applicable to other **HAN** syntheses which struggle with metal contaminants. Solid **HAN** is ideal for cocrystallization, and purification from metal contaminants ensures thermal analysis uncomplicated by catalytic decomposition, an important consideration for applications in propellants. Rapid cocrystal screening can be achieved via melt fusion of solid **HAN**, bypassing complex solution methods which must be adjusted to suit the needs of individual coformers. Through this method, the first set of **HAN** cocrystals have been reported. Eight of nine cocrystals have reduced hygroscopicity to the point of remaining stable as solids under ambient conditions, and one cocrystal, **HAN:PA**, eliminates the hygroscopicity of **HAN** entirely. The ability to stabilize **HAN** such that it is easily handled under ambient conditions without significant moisture uptake should enable research on **HAN** in the context of solid propellants, where it has not previously been studied in spite of its excellent oxygen content and existing production infrastructure. **HAN:ANTA**, **HAN:5-AT**, and **2HAN:PDO** possess noteworthy energetic properties exceeding those of both **HAN** and the coformer molecules. Ionic cocrystallization of oxidizing salts with organic coformers necessarily results in reduced oxygen balance, and while the cocrystals presented are no exception, incorporation of more oxygen-rich coformers or ones which can accommodate greater stoichiometric quantities of oxidizer in future work may mitigate the impact to oxidizing power as demonstrated in previous work with **AN** and **ADN**. While thermal stability remains a challenge, every cocrystal assessed shows a marked improvement over **HAN** in that regard. The potential of ionic cocrystallization as a route towards addressing the undesirable properties of **HAN** and thus enabling it for further study in solid applications is clearly demonstrated.

Author contributions

Andrew J. Bennett conceived research, designed experiments, performed experimental work and drafted the manuscript; Haley R. Froberg and Leila M. Foroughi performed experimental work and edited the manuscript; Michael K. Bellas conceived research and edited the manuscript; Adam J. Matzger

Open Access Article. Published on 06 January 2026. Downloaded on 5/24/2026 8:23:32 PM. This article is licensed under a Creative Commons Attribution-NonCommercial 3.0 Unported Licence.

conceived research, edited the manuscript, and provided project administration, resources, and supervision.

Conflicts of interest

There are no conflicts to declare.

Data availability

Supplementary information (SI): experimental details, Raman spectra, powder X-ray patterns, crystallographic information, DSC and TGA thermograms, and ORTEP diagrams. See DOI: https://doi.org/10.1039/d5ta08279j.

CCDC 2483543–2483551 contain the supplementary crystallographic data for this paper.[51a–i]

Acknowledgements

This work was supported by the ONR (grant no. N00014-22-1-2101 and N00014-25-1-2207) and by a NASA Space Technology Graduate Research Opportunity (grant no. 80NSSC22K1182). The authors thank the Office of Naval Research for financial support through the In-House Laboratory Independent Research Program.

References

1 J. P. Agrawal in *High Energy Mater.*, John Wiley & Sons, Ltd, 2010, pp. 209–330.
2 F. J. C. Roe, G. A. Grant and D. M. Millican, Carcinogenicity of Hydrazine and 1,1-Dimethylhydrazine for Mouse Lung, *Nature*, 1967, **216**, 375–376.
3 E. H. Vernot, J. D. MacEwen, R. H. Bruner, C. C. Haun, E. R. Kinkead, D. E. Prentice, A. Hall, R. E. Schmidt, R. L. Eason, G. B. Hubbard and J. T. Young, Long-term inhalation toxicity of hydrazine, *Fundam. Appl. Toxicol.*, 1985, **5**, 1050–1064.
4 R. P. Singh, R. D. Verma, D. T. Meshri and J. M. Shreeve, Energetic Nitrogen-Rich Salts and Ionic Liquids, *Angew. Chem., Int. Ed.*, 2006, **45**, 3584–3601.
5 A. E. S. Nosseir, A. Cervone and A. Pasini, Review of State-of-the-Art Green Monopropellants: For Propulsion Systems Analysts and Designers, *Aerospace*, 2021, **8**, 20.
6 Q. Zhang and J. M. Shreeve, Energetic Ionic Liquids as Explosives and Propellant Fuels: A New Journey of Ionic Liquid Chemistry, *Chem. Rev.*, 2014, **114**, 10527–10574.
7 T. Zhou, C. Gui, L. Sun, Y. Hu, H. Lyu, Z. Wang, Z. Song and G. Yu, Energy Applications of Ionic Liquids: Recent Developments and Future Prospects, *Chem. Rev.*, 2023, **123**, 12170–12253.
8 A. Hui, L. Jinyi, Y. Lujun, L. Shengxue, Z. Yanhong, Y. Huan, J. Qingjun, C. Zhihong and C. Jia, Acute and subchronic toxicity of hydroxylammonium nitrate in Wistar rats, *J. Med. Coll. PLA*, 2008, **23**, 137–147.
9 T. Katsumi and K. Hori, Successful development of HAN based green propellant, *Energ. Mater. Front.*, 2021, **2**, 228–237.
10 R. Amrousse, T. Katsumi, N. Azuma and K. Hori, Hydroxylammonium nitrate (HAN)-based green propellant as alternative energy resource for potential hydrazine substitution: from lab scale to pilot plant scale-up, *Combust. Flame*, 2017, **176**, 334–348.
11 A. Witze, Green fuels blast off, *Nature*, 2013, **500**, 509–510.
12 K. Chung, E. Rozumov, D. Kaminsky, P. Anderson, P. Cook, W. Sawka, M. McPherson and T. Buescher, Development of Electrically Controlled Energetic Materials (ECEM), *ECS Trans.*, 2013, **50**, 59.
13 F. Li, Z. Wang, Q. Zhang, Z. Cheng, Y. Yu, R. Shen, Y. Ye, L. T. DeLuca and W. Zhang, Tuning combustion and energy in hydroxylammonium nitrate (HAN)-based electrically controlled solid propellant, *Chem. Eng. J.*, 2024, **487**, 150562.
14 G. Steinhauser and T. M. Klapötke, Green Pyrotechnics: A Chemists' Challenge, *Angew. Chem., Int. Ed.*, 2008, **47**, 3330–3347.
15 D. Trache, T. M. Klapötke, L. Maiz, M. Abd-Elghany and L. T. DeLuca, Recent advances in new oxidizers for solid rocket propulsion, *Green Chem.*, 2017, **19**, 4711–4736.
16 J. Singh, R. J. Staples and J. M. Shreeve, Manipulating nitration and stabilization to achieve high energy, *Sci. Adv.*, 2023, **9**, eadk3754.
17 B. N. Kondrikov, V. É. Annikov, V. Yu. Egorshev and L. T. De Luca, Burning of hydroxylammonium nitrate, *Combust. Explos. Shock Waves*, 2000, **36**, 135–145.
18 C. Oommen and S. R. Jain, Ammonium nitrate: a promising rocket propellant oxidizer, *J. Hazard. Mater.*, 1999, **67**, 253–281.
19 F. Chen, C. Xuan, Q. Lu, L. Xiao, J. Yang, Y. Hu, G.-P. Zhang, Y. Wang, F. Zhao, G. Hao and W. Jiang, A review on the high energy oxidizer ammonium dinitramide: its synthesis, thermal decomposition, hygroscopicity, and application in energetic materials, *Def. Technol.*, 2023, **19**, 163–195.
20 J. C. Bottaro, P. E. Penwell and R. J. Schmitt, 1,1,3,3-Tetraoxo-1,2,3-triazapropene Anion, a New Oxy Anion of Nitrogen: The Dinitramide Anion and Its Salts, *J. Am. Chem. Soc.*, 1997, **119**, 9405–9410.
21 O. Elishav, B. M. Lis, E. M. Miller, D. J. Arent, A. Valera-Medina, A. G. Dana, G. E. Shter and G. S. Grader, Progress and Prospective of Nitrogen-Based Alternative Fuels, *Chem. Rev.*, 2020, **120**, 5352–5436.
22 M. K. Bellas and A. J. Matzger, Achieving Balanced Energetics through Cocrystallization, *Angew. Chem., Int. Ed.*, 2019, **58**, 17185–17188.
23 A. J. Bennett, L. M. Foroughi and A. J. Matzger, Perchlorate-Free Energetic Oxidizers Enabled by Ionic Cocrystallization, *J. Am. Chem. Soc.*, 2024, **146**, 1771–1775.
24 M. L. Levinthal, R. L. Willer, D. J. Park and R. Bridges, Process for Making High Purity Hydroxylammonium Nitrate, Utility, US5266290A, 1993.
25 T. Liggett, Hydroxylammonium Nitrate Process, Utility, US5182092A, 1993.
26 D. G. Harlow, R. E. Felt, S. Agnew, G. S. Barney, J. M. McKibben, R. Garber, M. Lewis, *Technical Report on Hydroxylamine Nitrate*, U.S. Department Of Energy, 1998.

 This journal is © The Royal Society of Chemistry 2026

Open Access Article. Published on 06 January 2026. Downloaded on 5/24/2026 8:23:32 PM. This article is licensed under a Creative Commons Attribution-NonCommercial 3.0 Unported Licence.

27 J. I. Artman and J. B. Ott, Solid + liquid phase equilibria in the hydroxylammonium nitrate + water system, *J. Energ. Mater.*, 1989, **7**, 115–132.
28 M. Guo, X. Sun, J. Chen and T. Cai, Pharmaceutical cocrystals: a review of preparations, physicochemical properties and applications, *Acta Pharm. Sin. B*, 2021, **11**, 2537–2564.
29 E. J. Broemmelsiek, J. L. Rovey and S. P. Berg, Effect of Metal Sequestrants on the Decomposition of Hydroxylammonium Nitrate, *Catalysts*, 2021, **11**, 1488.
30 S. Hoyani, R. Patel, C. Oommen and R. Rajeev, Thermal stability of hydroxylammonium nitrate (HAN): role of preparatory routes, *J. Therm. Anal. Calorim.*, 2017, **129**, 1083–1093.
31 E. W. Schmidt, *Hydroxylammonium Nitrate Compatibility Tests with Various Materials - A Liquid Propellant Study*, Rocket Research Company, 1990.
32 CDC, *NIOSH Pocket Guide to Chemical Hazards - Barium Sulfate*, https://www.cdc.gov/niosh/npg/npgd0047.html, accessed 19 June 2025.
33 CDC, *NIOSH Pocket Guide to Chemical Hazards - Calcium Sulfate*, https://www.cdc.gov/niosh/npg/npgd0095.html, accessed 19 June 2025.
34 S. Jia, Z. Gao, N. Tian, Z. Li, J. Gong, J. Wang and S. Rohani, Review of melt crystallization in the pharmaceutical field, towards crystal engineering and continuous process development, *Chem. Eng. Res. Des.*, 2021, **166**, 268–280.
35 G. Bolla, B. Sarma and A. K. Nangia, Crystal Engineering of Pharmaceutical Cocrystals in the Discovery and Development of Improved Drugs, *Chem. Rev.*, 2022, **122**, 11514–11603.
36 S. Li, T. Yu, Y. Tian, C. Lagan, D. S. Jones and G. P. Andrews, Mechanochemical Synthesis of Pharmaceutical Cocrystal Suspensions via Hot Melt Extrusion: Enhancing Cocrystal Yield, *Mol. Pharm.*, 2018, **15**, 3741–3754.
37 L. M. Foroughi, A. J. Bennett, J. L. Yeh and A. J. Matzger, Hydroxylammonium Chloride Cocrystals: Structural and Hygroscopicity Trends, *Cryst. Growth Des.*, 2025, **25**(19), 7903–7910.
38 A. J. Cruz-Cabeza, Acid–base crystalline complexes and the pKa rule, *CrystEngComm*, 2012, **14**, 6362–6365.
39 M. K. Bellas, L. V. MacKenzie and A. J. Matzger, Lamellar Architecture Affords Salt Cocrystals with Tunable Stoichiometry, *Cryst. Growth Des.*, 2021, **21**, 3540–3546.
40 A. K. Sikder, M. Geetha, D. B. Sarwade and J. P. Agrawal, Studies on characterisation and thermal behaviour of 3-amino-5-nitro-1,2,4-triazole and its derivatives, *J. Hazard. Mater.*, 2001, **82**, 1–12.
41 T. D. Manship, D. M. Smith and D. G. Piercey, An Improved Synthesis of the Insensitive Energetic Material 3-Amino-5-Nitro-1,2,4-triazole (ANTA), *Propellants, Explos. Pyrotech.*, 2020, **45**, 1621–1626.
42 T. M. Klapötke, *Chemistry of High-Energy Materials*, De Gruyter, 2017.
43 L. Bao, H. Wang, T. Zheng, S. Chen, W. Zhang, X. Zhang, Y. Huang, R. Shen and Y. Ye, Exploring the Influences of Conductive Graphite on Hydroxylammonium Nitrate (HAN)-Based Electrically Controlled Solid Propellant, *Propellants, Explos. Pyrotech.*, 2020, **45**, 1790–1798.
44 J. J. Sabatini, E.-C. Koch, J. C. Poret, J. D. Moretti and S. M. Harbol, Chlorine-Free Red-Burning Pyrotechnics, *Angew. Chem., Int. Ed.*, 2015, **54**, 10968–10970.
45 K. A. Monogarov, I. N. Melnikov, I. A. Vatsadze, I. L. Dalinger, I. V. Ananyev and N. V. Muravyev, Pyrazine 1,4-Dioxide is a Prolific Cocrystal Former and Energetic Material Itself, *Cryst. Growth Des.*, 2024, **24**, 741–746.
46 W. Kaim, The Versatile Chemistry of 1,4-Diazines: Organic, Inorganic and Biochemical Aspects, *Angew Chem. Int. Ed. Engl.*, 1983, **22**, 171–190.
47 S. T. Nicolau and A. J. Matzger, Sensitizing Explosives Through Molecular Doping, *ChemPlusChem*, 2024, **89**, e202300724.
48 M. K. Bellas and A. J. Matzger, Achieving Balanced Energetics through Cocrystallization, *Angew. Chem.*, 2019, **131**, 17345–17348.
49 K. Inoue, S. Matsumoto and M. Kumasaki, Preparation and crystallographic characterization of 1H-tetrazole/NaClO4 energetic cocrystal, *Acta Crystallogr., Sect. B:Struct. Sci., Cryst. Eng. Mater.*, 2022, **78**, 876–883.
50 K. B. Landenberger, O. Bolton and A. J. Matzger, Energetic–Energetic Cocrystals of Diacetone Diperoxide (DADP): Dramatic and Divergent Sensitivity Modifications via Cocrystallization, *J. Am. Chem. Soc.*, 2015, **137**, 5074–5079.
51 (*a*) CCDC 2483543: Experimental Crystal Structure Determination, 2026, DOI: 10.5517/ccdc.csd.cc2pcb9q.; (*b*) CCDC 2483544: Experimental Crystal Structure Determination, 2026, DOI: 10.5517/ccdc.csd.cc2pcbbr; (*c*) CCDC 2483545: Experimental Crystal Structure Determination, 2026, DOI: 10.5517/ccdc.csd.cc2pcbcs; (*d*) CCDC 2483546: Experimental Crystal Structure Determination, 2026, DOI: 10.5517/ccdc.csd.cc2pcbdt; (*e*) CCDC 2483547: Experimental Crystal Structure Determination, 2026, DOI: 10.5517/ccdc.csd.cc2pcbfv; (*f*) CCDC 2483548: Experimental Crystal Structure Determination, 2026, DOI: 10.5517/ccdc.csd.cc2pcbgw; (*g*) CCDC 2483549: Experimental Crystal Structure Determination, 2026, DOI: 10.5517/ccdc.csd.cc2pcbhx; (*h*) CCDC 2483550: Experimental Crystal Structure Determination, 2026, DOI: 10.5517/ccdc.csd.cc2pcbjy; (*i*) CCDC 2483551: Experimental Crystal Structure Determination, 2026, DOI: 10.5517/ccdc.csd.cc2pcbkz.